Journal of Mathematical Biology manuscript No.
(will be inserted by the editor)

Numerical rate function determination in partial differential equations modeling cell population dynamics

A. Groh · H. Kohr · A. K. Louis

Received: 18 Aug 2014 / Accepted: 30 May 2016

Abstract This paper introduces a method to solve the inverse problem of determining an unknown rate function in a partial differential equation (PDE) based on discrete measurements of the modeled quantity. The focus is put on a size-structured population balance equation (PBE) predicting the evolution of the number distribution of a single cell population as a function of the size variable.
Since the inverse problem at hand is ill-posed, an adequate regularization scheme is required to avoid amplification of measurement errors in the solution method. The technique developed in this work to determine a rate function in a PBE is based on the approximate inverse method, a pointwise regularization scheme, which employs two key ideas. Firstly, the mollification in the directions of time and size variables are separated. Secondly, instable

Andreas Groh
Hexagon Metrology PTS
Walter-Zapp-Strasse 4
35578 Wetzlar, Germany
Tel.: +49-6441 2109-206
Fax: +49-6441 2109-109
E-mail: andreas.groh@hexagonmetrology.com

Holger Kohr
Royal Institute of Technology (KTH)
Lindstedtsvägen 25
10044 Stockholm, Sweden
Tel.: +46-8 790-7320
Fax: +46-8 723-1788
E-mail: kohr@kth.se

Alfred K. Louis
Saarland University
POB: 151150
66041 Saarbrücken, Germany
Tel.: +49-681 302-3018
Fax: +49-681 302-4435
E-mail: louis@num.uni-sb.de

numerical data derivatives are circumvented by shifting the differentiation to an analytically given function.
To examine the performance of the introduced scheme, adapted test scenarios have been designed with different levels of data disturbance simulating the model and measurement errors in practice. The success of the method is substantiated by visualizing the results of these numerical experiments.

Keywords Inverse problem · Cell population dynamics · Partial differential equation · Parameter estimation · Population balance equation

Mathematics Subject Classification (2000) 65M32 · 92D25 · 47A52

1 Introduction

In general, a size-structured population balance equation (PBE) models the temporal evolution of a number distribution of particles as a function of a 'size' variable (Ramkrishna, 2000). In a biological context, the modeled entities are single cells, and the size variable usually reflects an intracellular state, e.g., cell volume, cell mass or DNA content (Henson, 2003). The usage of a PBE to model the evolution of a cell number distribution goes back to pioneering papers published about 50 years ago (Eakman et al., 1966; Tsuchiya et al., 1966; Bell and Anderson, 1967; Fredrickson et al., 1967; Sinko and Streifer, 1967; Bell, 1968; Ramkrishna et al., 1968; Anderson et al., 1969; Sinko and Streifer, 1969; Subramanian et al., 1970; Sinko and Streifer, 1971). There have been many generalizations and enhancements since then, for instance by Metz and Diekmann (1986), Henson (2003), Sidoli et al. (2004) or Webb (2008). The articles by Arino (1995) and Gyllenberg (2007) provide a brief history of (size) structured PBEs. The first mathematically rigorous treatment of this class of equations was elaborated by Diekmann et al. (1984); see also Diekmann et al. (1983) and Heijmans (1984).
In this paper, the following PBE serves as a base for the investigation of the inverse problem:

$$\underbrace{\partial_t n(t,x)}_{\text{accumulation}} + \underbrace{\partial_x\Big(c(x)\,n(t,x)\Big)}_{\text{cell growth}} + \underbrace{b(x)\,n(t,x)}_{\text{division}} = \underbrace{2\int_x^\infty b(\xi)\,q(x,\xi)\,n(t,\xi)\,\mathrm{d}\xi}_{\text{birth}}, \qquad t,x>0. \tag{1}$$

This equation or its special cases have been considered by most of the above cited works. It has been particularly developed to model cell division, other growth or fragmentation processes as in polymeres require modifications. In (1), $n(t,x)$ represents the number of cells with size x at time t. In general, the function $c \geq 0$ in the second term additionally depends on a nutrient concentration (Henson, 2003) which is assumed to be constant in this paper. In literature, c is referred to as *growth rate* having the dimension of size per time unit (Ramkrishna, 2000). The *fission* or *birth rate* b is a frequency with SI unit

$\left[\mathrm{s}^{-1}\right]$. Finally, the partitioning function q describes the statistical distribution of the mother cells content to the two daughter cells. Its unit is inverse to the considered size dimension, i.e., $\left[\mathrm{kg}^{-1}\right]$ or $\left[\mathrm{m}^{-1}\right]$. To avoid unit considerations, a nondimensionalization is carried out by scaling t and x by reference quantities and substituting the functions n, c, b and q in (1) accordingly. In the following, it is assumed that such a nondimensionalization has been applied. In order to achieve uniqueness, (1) is supplemented with adequate initial and boundary conditions,

$$n(0,x) = n_0(x)\ ,\ x > 0, \tag{2}$$

$$n(t,0) = 0\ ,\ t > 0. \tag{3}$$

It has been proven under quite general conditions that for fixed x the solution $n(t,x)$ of the system (1)–(3) grows asymptotically like $e^{\lambda t}$ for $t \to \infty$. In a biological context, the positive constant λ is referred to as *Malthus parameter*. Details concerning the asymptotic behavior in the general case have been investigated by Doumic-Jauffret and Gabriel (2010); for specific cases see the articles by Michel et al. (2005), Perthame and Ryzhik (2005) or Laurençot and Perthame (2009) as well as the book by Perthame (2006).

According to Doumic-Jauffret and Tine (2011), the functions c and q in (1) can be determined experimentally, in contrast to the birth rate b. Therefore, the current paper aims at developing an algorithm to approximate b for given c, q and n_0, where measurements of n serve as input. This data consists of histograms of the number distribution being measured at several points in time by a *cell flow cytometer* (Abu-Absi et al., 2003; Liu et al., 2007; Banks et al., 2011).

From a biological viewpoint, the knowledge about the birth rate is crucial for two reasons. Firstly, if all coefficient functions are known, the direct problem can be solved. This means that the system (1)–(3) can be used to predict the evolution of a cell population in a real application. Secondly, the determination of b from real data sets can be used to validate model assumptions concerning the shape of this function.

Inverse problems of this type automatically arise in biological, medical or biotechnological applications. The common task of these problems is to find rate functions or parameters in an equation modeling the evolution of a cell population. Several references in connection with structured PBEs that focus on rate determination in order to fit real data sets are provided by Mancuso et al. (2010a). Recently, cell number distributions of *human umbilical vein endothelial cells* have been used to approximate variable coefficients in a PBE of the form (1), and moreover, the influence of different drug additions has been analyzed (Mancuso et al., 2010b). Banks et al. (2011) employ a simplified version of (1) to model the dynamics of *human peripheral blood mononuclear cells* and, based on flow cytometry data of this cell line, determine the proliferation as well as the death rate. A similar problem in immunology has been considered by Luzyanina et al. (2007) who also emphasize the necessity of schemes to reconstruct unknown quantities in PBEs in order to provide a more thorough

understanding of cellular processes. In a recent paper by Kolewe et al. (2012), equation (1) has been employed to model aggregation dynamics of *taxus* cell cultures. This application in botanics aims at adjusting a parameter set in order to fit the simulated data to the measurements. Its goal is to understand the intra- and intercellular relations helping to control and optimize processes in biotechnological engineering. Further usages of structured PBEs can be found in articles by Henson (2003), Sidoli et al. (2004) and Doumic et al. (2010).
These are just a few examples from a biological context that underline the importance of the development of efficient and stable schemes to compute unknown rate functions in PBEs of the type (1) or certain variations. A standard solution technique would be the discretization of the searched-for function followed by a least squares approach, which can be handled by optimization routines. Depending on the resolution of the approximation, this procedure usually leads to high-dimensional minimization problems, the solution of which can produce inaccurate results or consume a lot of time. The developed novel method in this paper differs entirely from this well-known concept. Though being a significant enhancement of the basic algorithm developed by Groh et al. (2011), it still has potential for several generalizations which will be explained in detail later on.
The solution of inverse problems in connection with structured PBEs has been pioneered by Rundell (1989, 1993), Pilant and Rundell (1991a,b) and Engl et al. (1994) in a series of publications. All these papers deal with age-structured cell population dynamics modeled by first order hyperbolic PDEs. The structure of that type of equations differs somewhat from the PBE in this paper, yet the determination of the searched-for rate function requires an adequate regularization as well if noisy data serve as input. An inverse problem of age-structured population dynamics that involves cell reproduction by fission has been investigated by Gyllenberg et al. (2002, 2003).
Before going into details how the birth rate can be approximated, a brief summary of the investigated problem and the proposed solution method is expounded in the following. The considered PBE can be written in the form

$$\mathcal{A}(bn) = \mathcal{D}n, \tag{4}$$

where n is assumed to be given and b is the searched-for rate function. In (4), the operator $\mathcal{A}$ is of dilation type, and $\mathcal{D}$ represents a first order differential operator. This equation can be further condensed to

$$\mathcal{A}f = g \tag{5}$$

with *auxiliary function* $f = bn$ and *data function* $g = \mathcal{D}n$. The employed *approximate inverse method* generates an approximation f_γ to the solution of (5), which can be written as inner product of g with a calculable function Ψ_γ^x, the so-called *reconstruction kernel*:

$$f_\gamma : x \mapsto \left\langle \Psi_\gamma^x, g \right\rangle .$$

This representation opens up the possibility for the consecutive step. Its key idea is to insert the definition of g and shift the differential operator from n to Ψ_γ by employing the properties of the inner product,

$$f_\gamma : x \mapsto \left\langle \Psi_\gamma^x, g \right\rangle = \left\langle \Psi_\gamma^x, \mathcal{D}n \right\rangle = \left\langle \mathcal{D}^* \Psi_\gamma^x, n \right\rangle, \tag{6}$$

where $\mathcal{D}^*$ denotes the dual operator of $\mathcal{D}$.
In practice, n can be measured only at finitely many points, and the values are corrupted with noise. Avoiding the differentiation of n according to (6) implies a considerable improvement of stability and thus of the solution quality. As mentioned above, the actual task is to determine b which can be achieved by employing the relation

$$b\, n = f \approx f_\gamma.$$

If the auxiliary function f_γ has been determined, b can be simply calculated by pointwise division of f_γ by n. However, for data points $n \approx 0$ this naive approach should be avoided.
All techniques to solve the particular problems of the single solution steps are detailed in this paper, which is organized as follows. Subsequent to this introduction, the investigated inverse problem is precisely formulated and abstracted in a general notation. Section 3 presents the concept of the approximate inverse method which serves as a base for the developed reconstruction algorithm. The following Section 4 addresses the theoretical analysis of the inverse problem and introduces appropriate function spaces. Section 5 elaborates the reconstruction method leading to Theorem 1 providing an explicit characterization of the regularized solution where the instable differentiation of the data function is circumvented. Section 6 establishes the regularization property of the proposed method as well as convergence rates with respect to the data error. Concluding the algorithmic part, Section 7 covers some practice-oriented implementation issues. Subsequent to the introduction of the test problems, Section 8 illustrates and analyzes the numerical reconstructions for different scenarios and parameter choices. Finally, Section 9 draws conclusions from the results and provides an outlook on upcoming projects.

2 Problem formulation

Basically, this paper covers the inverse problem of determining the unknown rate function arising in a PBE that models cell population dynamics under the assumption of *equal partitioning* as considered by Arino (1995), Sidoli et al. (2004) and Perthame (2006). This means that during fission, the size of a mother cell is equally distributed to the two daughter cells. In consequence, the integral term in (1) simplifies to a dilation term:

$$\begin{aligned} \partial_t n(t,x) + \partial_x \Big(c(x)\, n(t,x) \Big) + b(x)\, n(t,x) = 4b(2x)\, n(t,2x), \\ x \geq 0,\ t \geq 0. \end{aligned} \tag{7}$$

This approach has been widely employed to model equal mitosis, e.g., by Sinko and Streifer (1971), Diekmann (1984), Diekmann et al. (1984), Liou et al. (1997) and Perthame (2006). Theorem 4.3 in the book by Perthame (2006) states that the system (7), (2), (3) has a unique solution $n \geq 0$ with

$$\|n(t,\cdot)\|_{L^1(\mathbb{R}^+)} = \int_0^\infty n(t,x)\,\mathrm{d}x \leq \|n_0\|_{L^1(\mathbb{R}^+)}\ \exp\left(B\,t\right) \tag{8}$$

where $B = \|b\|_{L^\infty(\mathbb{R}^+)}$. This estimate suggests that an L^1 setting is a suitable framework to study this inverse problem. Further results on regularity and L^∞ estimates can be found in Section 4.2.1. of the same book as well as in articles by Michel et al. (2005), Perthame and Ryzhik (2005), Michel (2006a,b), Perthame and Zubelli (2007) and Laurençot and Perthame (2009). In analogy to Michel et al. (2005) or Doumic (2007), the PBE (7) is generalized by considering a time-dependent birth rate $b(t,x)$. In most models concerning cell division, it suffices to assume that the birth rate is a function of the scalar size variable only, $b : \mathbb{R}^+ \to \mathbb{R}^+$. However, the univariate case is obviously included in the general case examined here. Consequently, the system investigated in this paper reads as

$$\begin{aligned} 4b(t,2x)\,n(t,2x) - b(t,x)\,n(t,x) = \partial_t n(t,x) + \partial_x\Big(c(x)\,n(t,x)\Big), \\ x \geq 0,\ t \geq 0, \end{aligned} \tag{9}$$

$$n(t,0) = 0, \qquad t > 0, \tag{10}$$

$$n(0,x) = n_0(x),\ x > 0. \tag{11}$$

Following the strategy of Groh et al. (2011), an auxiliary function f is defined as $f(t,x) = b(t,x)n(t,x)$. Likewise, the data terms are combined to a function

$$g(t,x) = D_c n(t,x) \tag{12}$$

with the linear differential operator

$$D_c = \partial_t + \partial_x c. \tag{13}$$

Furthermore, let I denote the identity and

$$Tf(t,x) = 4f(t,2x) \tag{14}$$

the multiple of a dilation in the size variable. The operator $\mathcal{A}$ is defined by

$$\mathcal{A} = T - I \tag{15}$$

and the primary task is to solve $\mathcal{A}f(t,x) = g(t,x)$. The analogous inverse problem focusing on the corresponding steady state equation of (9), has first been considered by Perthame and Zubelli (2007). For $c = 1$, the equation for the stable cell number distribution N reads as

$$4b(2x)N(2x) - b(x)N(x) = N'(x) + \lambda N(x), \tag{16}$$

where b is the birth rate and $\lambda > 0$ the Malthus parameter as before. Obviously, by defining $\tilde{f}(x) = b(x)N(x)$, the same dilation operator as in (15) emerges. Moreover, both the data function (12) and the right hand side of (16) involve derivatives of the number distribution, hence the problem statements are similar.
It has been shown by Perthame and Zubelli (2007) that under the regularity condition $N' \in L^p(\mathbb{R}^+)$ for $p \geq 1$, the problem of determining b in (16) is well-posed. They further argue that the aforementioned regularity of N cannot be assumed due to the unavoidable measurement errors, and therefore the data N is merely expected to lie in L^p. An analogous analysis of the inverse problem and its regularization has been continued by Doumic et al. (2010), Doumic-Jauffret and Tine (2011) and Doumic-Jauffret et al. (2012) for more general PBEs, i.e., with integral term and non-constant growth rate c.
Prior to the introduction of the solution technique, the inverse problem is analysed with regard to appropriate function spaces and mapping properties of the involved operators.

3 Approximate inverse method

Let $A : X \to Y$ be a bounded linear operator between two Banach spaces X and Y of functions on a domain $\Omega \subset \mathbb{R}^d$. The task is to solve the equation $Af = g$ for a given function $g \in Y$. In practice, the problem of determining f is usually ill-posed, and therefore an adequate regularization is required (Louis, 1989). The *approximate inverse method*, being a pointwise regularization scheme, is based on two key ideas (Louis, 1996, 2011; Schuster, 2007; Schuster and Schöpfer, 2010).
Firstly, the sought-for function f is replaced with f_γ defined by $f_\gamma(x) = \langle f, \delta_\gamma^x \rangle$. In this definition, the square brackets denote the dual product on $X \times X^*$, and the so-called *mollifier* δ_γ^x represents an approximation of δ^x, the *Dirac delta distribution* for the point x. To be more precise, δ_γ^x has to fulfill the condition that for all $f \in X$, the approximate version f_γ is an element of X and converges to f with respect to the norm on X for $\gamma \to 0$.
Secondly, δ_γ^x is employed to define an auxiliary problem

$$A^* \psi_\gamma^x = \delta_\gamma^x, \tag{17}$$

where A^* denotes the dual operator of A. In the special case of X and Y being Hilbert spaces, A^* is the usual adjoint. It can easily be verified that then

$$\langle g, \psi_\gamma^x \rangle = \langle Af, \psi_\gamma^x \rangle = \langle f, A^* \psi_\gamma^x \rangle = \langle f, \delta_\gamma^x \rangle = f_\gamma(x). \tag{18}$$

Thus, f_γ can be written as an inner product of the data g with the function ψ_γ^x referred to as *reconstruction kernel*. As a solution of (17), it is solely characterized by A^* and δ_γ^x and does therefore not depend on the data. Consequently, this quantity can be pre-calculated and, according to (18), merely the dual product $\langle g, \psi_\gamma^x \rangle$ has to be evaluated in order to compute a regularized solution $f_\gamma(x) \approx f(x)$.

The application of the delineated technique to the current problem requires adequate reformulations. The idea is to take advantage of a separation approach and to apply the algorithms developed by Groh et al. (2011) to each factor separately. This strategy is elaborated in detail in Section 5.

4 Analysis of the inverse problem

As mentioned above, the crucial step is to determine f as the solution of

$$(T - I)f = D_c n, \tag{19}$$

where T and D_c are given by (14) and (13), respectively. In the following, the properties of the operator T are investigated. Since T acts merely on the x-variable, the time dependence is dropped for the sake of readability readability,

$$(T - I) : L^1(\mathbb{R}^+) \longrightarrow L^1(\mathbb{R}^+), \quad (T - I)\phi(x) = 4\phi(2x) - \phi(x).$$

Lemma 1 *The inverse operator* $(T - I)^{-1} : L^1(\mathbb{R}^+) \to L^1(\mathbb{R}^+)$ *exists and is bounded with*

$$\left\| (T - I)^{-1} \right\|_{L^1(\mathbb{R}^+) \to L^1(\mathbb{R}^+)} \leq 1. \tag{20}$$

Proof Obviously, the inverse of $Tf(x) = 4f(2x)$ is

$$T^{-1} : L^1(\mathbb{R}^+) \longrightarrow L^1(\mathbb{R}^+), \quad T^{-1}\phi(x) = \frac{1}{4}\phi\left(\frac{x}{2}\right).$$

The definition of the L^1 norm and a simple variable transformation gives

$$\left\|T^{-1}\phi\right\|_{L^1(\mathbb{R}^+)} = \frac{1}{4}\int_0^\infty \left|\phi\left(\frac{x}{2}\right)\right| \,\mathrm{d}x = \frac{1}{2}\int_0^\infty |\phi(x)| \,\mathrm{d}x = \frac{1}{2}\left\|\phi\right\|_{L^1(\mathbb{R}^+)}.$$

Thus, the operator norm of T^{-1} is equal to $1/2$, and the inverse of $I - T^{-1}$ is given by the Neumann series (Yosida, 1995)

$$\left(I - T^{-1}\right)^{-1} = \sum_{i=0}^{\infty} T^{-i}.$$

The application of T^{-1} on both sides yields the explicit representation

$$(T - I)^{-1} = \sum_{i=1}^{\infty} T^{-i}$$

and the geometric series gives the claimed estimate of the operator norm. ■

It follows immediately that for $f, g \in L^1(\mathbb{R}^+)$, the problem of solving the linear equation

$$(T - I)f = g$$

is well-posed. In (19), the right hand side is $D_c n$. Accordingly, the problem of determining $f(t,\cdot) = b(t,\cdot)n(t,\cdot) \in L^1(\mathbb{R}^+)$ is well-posed if $D_c n(t,\cdot) \in L^1(\mathbb{R}^+)$. Roughly speaking, this condition says that also the partial derivatives of n have to be L^1 functions with respect to x. In a precise mathematical formulation, this leads to the introduction of an appropriate Sobolev space as elaborated in the following.
For fixed x, $n(t,x)$ grows exponentially as a function of t (Perthame and Zubelli, 2007), thus this function is not integrable with respect to t on $\mathbb{R}^+$. Likewise, since all functions in (9) are continuous, $\partial_t n(\cdot,x)$ is also continuous but not integrable on $\mathbb{R}^+$. Instead, it is assumed that these functions are integrable on a finite time interval $[0,T]$ for some fixed $T > 0$. The corresponding function space is defined as the Sobolev space $W_T^{1,1} = W^{1,1}\big([0,T] \times \mathbb{R}^+\big)$ equipped with the norm

$$\|f\|_{W_T^{1,1}} = \sum_{|\alpha| \le 1} \|D^\alpha f\|_{L^1([0,T]\times\mathbb{R}^+)} .$$

Under the additional condition that c and c' are bounded, it follows immediately from Lemma 1 and the fact that $\mathcal{D}_c$ is a first order differential operator that the problem of determining f from $D_c n = (T - I)f$ is well-posed. In practice, however, such a regularity conjecture for the data function n is too strong due to unavoidable measurement errors, finite sampling sizes and other disturbances. The more reasonable assumption $n \in L^1(\mathbb{R}^+)$ leads to an ill-posed problem due to the data differentiation (Louis, 1989; Engl et al., 1996), hence an appropriate regularization has to be developed.
Furthermore, with regard to the original problem, the determination of the birth rate b, an additional difficulty arises. Obviously, once the auxiliary function $f = bn$ is determined, b can simply be calculated by pointwise division,

$$b(t,x) = f(t,x)/n(t,x). \tag{21}$$

It has been shown by Perthame and Zubelli (2007) that for every t, the values of $n(t,x)$ are rapidly decaying for large x,

$$\lim_{x\to\infty} n(t,x) = 0,$$

and the boundary condition stipulates $n(t,0) = 0$. From a theoretical point of view, this does not cause considerable problems since $b(t,\cdot) \in L^\infty(\mathbb{R}^+)$ and $f(t,\cdot)$ shows the same asymptotic behavior as $n(t,\cdot)$ for $t \to 0$ and for $t \to \infty$. However, with regard to the algorithm development in a discrete setting, these properties of n for $x \approx 0$ and for $x \to \infty$ have to be taken into account because in these regions small reconstructions errors of f can be enormously amplified if the nominator in (21) is close to 0.

5 Solution of the inverse problem

The preceding section has shown that a regularization scheme is required to stably solve

$$\mathcal{A}f = D_c n$$

with $\mathcal{A} = T - I$ for discrete and error-prone data n. In the following, the approximate inverse method as introduced in 3 is concretized to the current setting, and an analytical expression for the reconstruction kernel is derived. According to (17), the auxiliary problem reads as

$$\mathcal{A}^* \Psi_\gamma^{(t,x)} = \delta_\gamma^{(t,x)}, \quad t, x > 0 \tag{22}$$

and the mollified solution is

$$f_\gamma(t,x) = \left\langle D_c n, \Psi_\gamma^{(t,x)} \right\rangle_{L_T^1 \times L_T^\infty}, \tag{23}$$

where $L_T^1 = L^1\big([0,T] \times \mathbb{R}^+\big)$ with its dual being $L_T^\infty = L^\infty\big([0,T] \times \mathbb{R}^+\big)$. An elementary calculation yields that the dual operator $\mathcal{A}^*$ is given by

$$\mathcal{A}^* v = (T^* - I)v \quad \text{with} \quad T^* v(t,x) = 2v\left(t, \frac{x}{2}\right).$$

Obviously, $\mathcal{A}$ and $\mathcal{A}^*$ act only on the size variable which motivates the following separation approach

$$\Psi^{(t,x)}(\tau,\xi) = \Psi_{\gamma_1}^t(\tau)\Psi_{\gamma_2}^x(\xi) \quad , \quad \delta^{(t,x)}(\tau,\xi) = \delta_{\gamma_1}^t(\tau)\delta_{\gamma_2}^x(\xi). \tag{24}$$

Inserting into (22) and sorting the terms gives

$$\Psi_{\gamma_1}^t(\tau) A^* \Psi_{\gamma_2}^x(\xi) = \delta_{\gamma_1}^t(\tau)\delta_{\gamma_2}^x(\xi)$$

with A standing for the time-independent version of $\mathcal{A}$. Comparison of the factors yields

$$\Psi_{\gamma_1}^t(\tau) = \delta_{\gamma_1}^t(\tau)$$

and the univariate equation

$$A^* \Psi_{\gamma_2}^x(\xi) = \delta_{\gamma_2}^x(\xi). \tag{25}$$

Lemma 2 *The inverse operator $A^{-*} = (T^* - I)^{-1} : L^\infty(\mathbb{R}^+) \to L^\infty(\mathbb{R}^+)$ exists and is given by*

$$A^{-*} v(x) = \sum_{k=1}^{\infty} 2^{-k} v\left(2^k x\right).$$

Proof The operator A^* can be factorized as

$$T^* - I = T^*\big(I - T^{-*}\big). \tag{26}$$

It is easy to see that the inverse of T^* is $T^{-*}v(x) = \frac{1}{2}v\,(2x)$. Since obviously, $\big\|T^{-*}\big\| = 1/2$, the inverse of $\big(I - T^{-*}\big)$ is given by the Neumann series

$$\big(I - T^{-*}\big)^{-1} = \sum_{k=0}^{\infty} (T^*)^{-k}$$

and (26) and the definition of T^* conclude the proof. ■

Let now the one-dimensional mollifiers for both t and x, respectively, be of *convolution type*, i.e. of the form

$$\delta_\gamma^x(\xi) = \delta_\gamma(x-\xi) = \gamma^{-1}\,\bar\delta\left(\frac{x-\xi}{\gamma}\right). \tag{27}$$

For simplicity, it is assumed that the same *generating function* $\bar\delta \in L^1(\mathbb{R})$ is used for both variables. This relation can be written in short as $\delta_\gamma^x = \mathcal{T}^x\delta^\gamma = \gamma^{-1}\mathcal{T}^x\mathcal{D}^\gamma\bar\delta$ with the *translation* and *dilation* operators

$$\mathcal{T}^x f(\xi) = f(x-\xi) \quad \text{and} \quad \mathcal{D}^\gamma f(x) = f(\gamma^{-1}x). \tag{28}$$

From Lemma 2, it follows immediately that

$$\Psi_{\gamma_2}^x(\xi) = \sum_{k=1}^{\infty} 2^{-k}\delta_{\gamma_2}^x\left(2^k\xi\right) = \sum_{k=1}^{\infty} 2^{-k}\delta_{\gamma_2}\left(x - 2^k\xi\right), \tag{29}$$

and that the approximate solution (23) is also given by a convolution:

$$f_\gamma(t,x) = \left\langle D_c n, \delta_{\gamma_1}^t \Psi_{\gamma_2}^x \right\rangle_{L_T^1 \times L_T^\infty} = \int_0^T \int_0^\infty D_c n(\tau,\xi)\,\delta_{\gamma_1}(t-\tau)\,\Psi_{\gamma_2}(x-\xi)\,\mathrm{d}\xi\,\mathrm{d}\tau. \tag{30}$$

In the inner integral, the derivative part of the operator D_c can be shifted to δ_{γ_1} and Ψ_{γ_2} by means of integration by parts. Furthermore, to make the above calculation rigorous, the integral kernel must have a certain regularity. Both aspects are addressed in the following theorem.

Theorem 1 *Let the generating function $\bar\delta$ of both mollifiers $\delta_{\gamma_1}^t$ and $\delta_{\gamma_2}^x$ be an element of the Sobolev space $W^{1,1}(\mathbb{R})$. Then the convolution kernel $\Psi_\gamma(t,x) = \delta_{\gamma_1}(t)\Psi_{\gamma_2}(x)$ in (30) satisfies $\Psi_\gamma \in W^{1,1}([0,T]\times\mathbb{R}^+)$. Furthermore, the approximate solution f_γ lies in L_T^1 and has the representation*

$$\begin{aligned} f_\gamma(t,x) = {} & \delta_{\gamma_1}(t-T)\int_0^\infty n_T(\xi)\,\Psi_{\gamma_2}(x-\xi)\,\mathrm{d}\xi - \delta_{\gamma_1}(t)\int_0^\infty n_0(\xi)\,\Psi_{\gamma_2}(x-\xi)\,\mathrm{d}\xi + \\ & \int_0^T\int_0^\infty n(\tau,\xi)\left(\delta_{\gamma_1}'(t-\tau)\,\Psi_{\gamma_2}(x-\xi) + c(\xi)\,\delta_{\gamma_1}(t-\tau)\,\Psi_{\gamma_2}(x-\xi)\right)\mathrm{d}\tau\,\mathrm{d}\xi, \end{aligned} \tag{31}$$

where $n_0 = n(0,\cdot)$ and $n_T = n(T,\cdot)$ are integrable functions on $\mathbb{R}^+$.

Proof Since $\bar{\delta} \in W^{1,1}(\mathbb{R})$, the temporal part δ_{γ_1} of the kernel and its derivative are integrable by definition. For the x part, it holds

$$\|\Psi_{\gamma_2}\|_{L^1} = \left\| \sum_{k=1}^{\infty} 2^{-k}\, \mathcal{D}^{2^{-k}} \delta_{\gamma_2} \right\|_{L^1} \leq \sum_{k=1}^{\infty} 2^{-2k} \|\delta_{\gamma_2}\|_{L^1} = \frac{1}{3} \|\bar{\delta}\|_{L^1} < \infty \tag{32}$$

since $\|\mathcal{D}^{\alpha} f\|_1 = \alpha \|f\|_1$, and further

$$\|\Psi'_{\gamma_2}\|_{L^1} = \left\| \sum_{k=1}^{\infty} \mathcal{D}^{2^{-k}} \delta'_{\gamma_2} \right\|_{L^1} \leq \sum_{k=1}^{\infty} 2^{-k} \|\delta'_{\gamma_2}\|_{L^1} = \gamma_2^{-1} \|\bar{\delta}'\|_{L^1} < \infty, \tag{33}$$

where the intertwining property $\partial_\xi \mathcal{D}^{\alpha} = \alpha^{-1} \mathcal{D}^{\alpha} \partial_\xi$ was used twice.
As far as the representation formula for f_γ is concerned, the t and x integrations in (30) can be treated separately due to $D_c = \partial_t + \partial_x c$ and the separation of the integral kernel. Regarding t, it is

$$\int_0^T \partial_\tau n(\tau,\xi)\, \delta_{\gamma_1}(t-\tau)\, \mathrm{d}\tau = n(T,\xi)\, \delta_{\gamma_1}(t-T) - n(0,\xi)\, \delta_{\gamma_1}(t) + \int_0^T n(\tau,\xi)\, \delta'_{\gamma_1}(t-\tau)\, \mathrm{d}\tau$$

With respect to x, the same argument together with the properties $n(\tau,0) = 0$ and $c(\xi)\, n(\tau,\xi)\, \Psi_{\gamma_2}(x-\xi) \to 0$ for $\xi \to \infty$ yields

$$\int_0^{\infty} \partial_\xi \big(c(\xi) n(\tau,\xi)\big)\, \Psi_{\gamma_2}(x-\xi)\, \mathrm{d}\xi = \int_0^{\infty} c(\xi)\, n(\tau,\xi)\, \Psi'_{\gamma_2}(x-\xi)\, \mathrm{d}\xi.$$

Since the convolution of integrable functions is again integrable, the proof is complete. ■

In practical applications, shifting the differentiation from the noisy data to the analytically given kernel can be expected to be beneficial in terms of stability. Furthermore, from the perspective of numerical implementation, a rapidly decaying generating function $\bar{\delta}$ has the advantage that the integrals can be truncated early. Groh et al. (2011) obtained good results with the Gaussian function, and this class of mollifiers is also appropriate for the current problem. However, numerical experiments have revealed that mollifiers with compact support can induce further improvements.

6 Regularization and convergence speed

The conditions under which the approximate inverse method acts as a regularization and shows a certain convergence rate in terms of the data error have been assessed in a number of articles for different settings, among others: L^2 using singular value decomposition (Louis and Maass, 1990), semi-discrete

Hilbert space setting (Rieder and Schuster, 2000, 2003), bounded linear operators on Banach spaces (Schuster and Schöpfer, 2010) and unbounded operators with data pre-processing (corresponding to $\mathcal{D}_c$ in this case) (Kohr, 2013). The proofs involve certain conditions on the mollifier and the calculated reconstruction kernel. In the following, this analysis is adapted to the current inverse problem.

6.1 Regularization

Given data $n^\epsilon \in L^1_T$ with $\|n - n^\epsilon\|_{L^1_T} < \epsilon$ and assuming $\mathcal{A}f = D_c n$, the task is to show that $\|f - \mathcal{A}^\gamma n^\epsilon\|_1$ vanishes for $\epsilon \to 0$ for an adequate parameter choice $\gamma = \gamma(\epsilon)$, where $\mathcal{A}^\gamma$ is defined by (31). The error can be split as

$$\begin{aligned}\|f - \mathcal{A}^\gamma n^\epsilon\|_{L^1_T} \le \|f - f_\gamma\|_{L^1_T} + \\ \|\mathcal{R}_1^\gamma(n - n^\epsilon)\|_{L^1_T} + \|\mathcal{R}_2^\gamma(n - n^\epsilon)\|_{L^1_T} + \|\mathcal{S}^\gamma(n - n^\epsilon)\|_{L^1_T},\end{aligned} \tag{34}$$

where the operators in the above estimate are defined as the three summands in the order they appear in (31). The point evaluation in the t variable for the operators $\mathcal{R}_1$ and $\mathcal{R}_2$ requires additional conditions since the inequality $\|n - n^\epsilon\|_{L^1_T} < \epsilon$ does not imply the corresponding inequalities for the functions $n(0,\cdot)$ and $n(T,\cdot)$. Due to their similarity, both terms can be analyzed in common as follows.

Lemma 3 *Let $\bar\delta \in W^{1,1}(\mathbb{R})$, and let $n_0 = n(0,\cdot)$ and $n_T = n(T,\cdot)$ fulfill*

$$\|n_0 - n_0^\epsilon\|_{L^1} \to 0 \quad \textit{and} \quad \|n_T - n_T^\epsilon\|_{L^1} \to 0 \quad \textit{for } \epsilon \to 0.$$

Then for any parameter choice $\gamma = \gamma(\epsilon) = (\gamma_1(\epsilon), \gamma_2(\epsilon))$, it holds

$$\lim_{\epsilon\to 0}\big\|\mathcal{R}_1^{\gamma(\epsilon)}(n - n^\epsilon)\big\|_{L_1^T} = \lim_{\epsilon\to 0}\big\|\mathcal{R}_2^{\gamma(\epsilon)}(n - n^\epsilon)\big\|_{L_1^T} = 0.$$

Proof For $\mathcal{R}_1$, it holds

$$\begin{aligned}\|\mathcal{R}_1^\gamma(n - n^\epsilon)\|_{L^1_T} &\le \|\delta_{\gamma_1}\|_{L^1}\,\big\|(n_T - n_T^\epsilon) * \Psi_{\gamma_2}\big\|_{L^1} \\ &\le \frac{1}{3}\|\bar\delta\|_{L^1}^2 \|n_T - n_T^\epsilon\|_{L^1}\end{aligned}$$

according to (32). The estimate for $\mathcal{R}_2$ can be proven with exactly the same argument. ∎

For the operator $\mathcal{S}^\gamma$, the following result can be obtained with similar techniques.

Lemma 4 *Let $\gamma = \gamma(\epsilon) = (\gamma_1(\epsilon), \gamma_2(\epsilon))$ be a parameter choice with the asymptotics $\gamma_j(\epsilon) \sim \epsilon^{s_j}$ for $\epsilon \to 0$ with $s_j < 1$ $(j = 1, 2)$. Then the error contribution of $\mathcal{S}^\gamma$ in (34) satisfies*

$$\lim_{\epsilon\to 0}\big\|\mathcal{S}^{\gamma(\epsilon)}(n - n^\epsilon)\big\|_{L_1^T} = 0.$$

Proof The operator $\mathcal{S}^\gamma$ can be written more compactly with the tensor product notation

$$(f_1 \otimes f_2)(t,x) = f_1(t)\, f_2(x) \quad \text{and} \quad (\mathcal{S} \otimes \mathcal{T})(f_1 \otimes f_2) \quad = (\mathcal{S} f_1) \otimes (\mathcal{T} f_2)$$

for functions and operators, respectively. It follows that

$$\begin{aligned}
\|S^\gamma(n - n^\epsilon)\|_{L^1_T} &\leq \|n - n^\epsilon\|_{L^1_T} \|\delta'_{\gamma_1} \otimes \Psi_{\gamma_2}\|_{L^1} + \|c(n - n^\epsilon)\|_{L^1_T} \|\delta_{\gamma_1} \otimes \Psi'_{\gamma_2}\|_{L^1} \\
&= \|n - n^\epsilon\|_{L^1_T} \|\delta'_{\gamma_1}\|_{L^1} \|\Psi_{\gamma_2}\|_{L^1} + \|c(n - n^\epsilon)\|_{L^1_T} \|\delta_{\gamma_1}\|_{L^1} \|\Psi'_{\gamma_2}\|_{L^1} \\
&= \|n - n^\epsilon\|_{L^1_T} \frac{1}{3} \gamma_1^{-1} \|\bar{\delta}'\|_{L^1} \|\bar{\delta}\|_{L^1} + \|c(n - n^\epsilon)\|_{L^1_T} \gamma_2^{-1} \|\bar{\delta}\|_{L^1} \|\bar{\delta}'\|_{L^1} \\
&\leq \max\{1, \|c\|_{L^\infty}\} \|\bar{\delta}\|_{L^1} \|\bar{\delta}'\|_{L^1} (\gamma_1^{-1} + \gamma_2^{-1}) \|n - n^\epsilon\|_{L^1_T}.
\end{aligned}$$

Since for the given parameter choice $\gamma(\epsilon)$, the factor $\gamma_1(\epsilon)^{-1} + \gamma_2(\epsilon)^{-1}$ grows slower than ϵ^{-1}, the above error term converges to zero for $\epsilon \to 0$. ■

The results of this section can be summarized in the following theorem.

Theorem 2 *Let $f \in L^1_T$ solve $\mathcal{A}f = \mathcal{D}_c n$ for $n \in W^{1,1}_T$. Let further $n^\epsilon \in L^1_T$ be the given data with*

$$\|n - n^\epsilon\|_{L^1_T} \leq \epsilon, \quad \|n_0 - n_0^\epsilon\|_{L^1} \leq \epsilon \quad \textit{and} \quad \|n_T - n_T^\epsilon\|_{L^1} \leq \epsilon.$$

If the parameter choice $\gamma(\epsilon) = (\gamma_1(\epsilon), \gamma_2(\epsilon))$ satisfies

$$\gamma_j(\epsilon) \sim \epsilon^{s_j} \quad \textit{for} \quad \epsilon \to 0 \quad \textit{with} \quad 0 < s_j < 1,\ j = 1, 2,$$

the approximate solution $f_{\gamma(\epsilon)}$ as defined in (31) *converges to f in L^1_T for $\epsilon \to 0$.*

Proof The positivity of the exponents s_j ensures that $\gamma_j(\epsilon) \to 0$ for $\epsilon \to 0$, and thus the approximation error $\|f - f_{\gamma(\epsilon)}\|_{L^1_T}$ vanishes in the limit of exact data. Together with Lemmas 3 and 4, this proves the claim.

6.2 Convergence speed

The qualitative statement of the previous section that the total reconstruction error tends to zero for $\epsilon \to 0$ can be made quantitative by studying the rate of this convergence. Since the error behavior the for data parts as analyzed in the Lemmas 3 and 4 is already given quantitatively, the only remaining part is the approximation error $\|f - f_{\gamma(\epsilon)}\|_{L^1_T}$. This term depends on the exact solution and the chosen mollifier but not (directly) on the data, hence the convergence rate can be adjusted by using mollifiers with certain properties.
Schuster and Schöpfer (2010) establish estimates of $\|f - f_\gamma\|$ in terms of powers of γ for the approximate inverse method in the case of L^p functions on compact sets. The assumption of compact support for the unknown function as well as for the mollifier is essential in their proof, and the argument cannot simply

be generalized for unbounded support. Therefore, a similar technique using slightly more careful estimates is presented here. The one-dimensional case is treated in detail, while only the key ideas for the generalization to the two-dimensional case are presented.

Lemma 5 *Let $f \in L^1(\mathbb{R}^+)$ decay as x^{-1-r} with $r > 0$ for $x \to \infty$. Furthermore, its continuation f_0 by zero to $\mathbb{R}$ be m-times continuously differentiable with bounded m-th derivative for some $m \geq 0$. Let additionally the generating function $\bar{\delta}$ of the one-dimensional mollifier fulfill the* moment conditions

$$\int_{\mathbb{R}} x^k \, \bar{\delta}(x) \, \mathrm{d}x = 0 \quad \textit{for } k = 1, \ldots, m-1, \tag{35}$$

$$\mu_k = \int_{\mathbb{R}} |x^k \, \bar{\delta}(x)| \, \mathrm{d}x < \infty \quad \textit{for } k = m, m+1. \tag{36}$$

Then the approximation error is of order m in γ.

Proof Due to the normalization property of the mollifier, it holds

$$\begin{aligned} f_\gamma(x) - f(x) &= \int_{\mathbb{R}^+} f(y) \, \delta_\gamma(x-y) \, \mathrm{d}y - f(x) \\ &= \int_{\mathbb{R}} \big(f_0(y) - f_0(x)\big) \, \delta_\gamma(x-y) \, \mathrm{d}y \\ &= \int_{\mathbb{R}} \bar{\delta}(z) \big(f_0(x-\gamma z) - f_0(x)\big) \, \mathrm{d}z. \end{aligned}$$

If the Taylor expansion of f_0 around x is inserted, all terms up to order $m-1$ in z vanish due to the property (35) of $\bar{\delta}$. Consequently, the approximation error can be written as

$$\|f_\gamma - f\|_{L^1(\mathbb{R}^+)} = \int_0^\infty \left| \int_{\mathbb{R}} \bar{\delta}(z) \frac{f_0^{(m)}(\bar{x})}{m!} \, (-\gamma z)^m \, \mathrm{d}z \right| \mathrm{d}x,$$

where $\bar{x}$ is some (unknown) point between x and $x - \gamma z$. The absolute value of $f_0^{(m)}(\bar{x})$ is smaller than its *modulus of continuity*

$$\omega\big(f_0^{(m)}; \gamma|z|, x\big) = \sup\Big\{ \big|f_0^{(m)}(y)\big| \;\Big|\; -\gamma|z| \leq x - y \leq \gamma|z| \Big\}. \tag{37}$$

Due to the decay condition of $f_0^{(m)}$, there are positive constants x_0 and α such that

$$\omega\big(f_0^{(m)}; \gamma|z|, x\big) \leq \begin{cases} \big\|f_0^{(m)}\big\|_{L^\infty}, & \text{if } x - \gamma|z| \leq x_0, \\ \alpha(x - \gamma|z|)^{-1-r}, & \text{if } x - \gamma|z| > x_0. \end{cases} \tag{38}$$

Hence, the approximation can be further estimated as

$$\|f_\gamma - f\|_{L^1(\mathbb{R}^+)} \leq \frac{\gamma^m}{m!} \int_{\mathbb{R}} |z^m \, \bar{\delta}(z)| \int_0^\infty \omega\big(f_0^{(m)}; \gamma|z|, x\big) \, \mathrm{d}x \, \mathrm{d}z,$$

and the inner integral fulfills

$$\begin{aligned}\int_0^\infty \omega\big(f_0^{(m)};\gamma|z|,x\big)\,\mathrm{d}x &\le \big\|f_0^{(m)}\big\|_{L^\infty}(x_0+\gamma|z|)+\alpha\int_{x_0}^\infty |x|^{-1-r}\,\mathrm{d}x\\ &= \big\|f_0^{(m)}\big\|_{L^\infty}(x_0+\gamma|z|)+\frac{\alpha}{r}\,x_0^{-r}.\end{aligned}$$

In consequence, the integral over z can be bounded in terms of $\big\|f_0^{(m)}\big\|_{L^\infty}$, r, α, x_0 and the moments μ_m and μ_{m+1}. This concludes the proof. ■

In the two-dimensional case, the arguments have to be modified only slightly. The following Lemma states the result, and the proof is merely sketched.

Lemma 6 *Let $f \in L^1_T$ decay as x^{-1-r} at infinity for some $r > 0$ in the sense that there exist positive constants x_0 and α independent of t such that $|f(t,x)| \le \alpha x^{-1-r}$ for all $x \ge x_0$. Furthermore, its continuation f_0 by zero to $\mathbb{R}^2$ be m-times continuously differentiable with bounded m-th derivative for some $m \ge 0$, and the mollifier satisfy the conditions of Lemma 5. Then it holds*

$$\|f - f_\gamma\|_{L^1_T} \le \textit{const.}\cdot(\gamma_1^m+\gamma_2^m),$$

where the constant depends on $\big\|f_0^{(m)}\big\|_{L^\infty}$, r, α, x_0 and the moments μ_m, μ_{m+1}.

Proof sketch The difference between f and f_γ is written as

$$\int_{\mathbb{R}^2} \bar\delta(z)\,\bar\delta(s)\big(f_0(t-\gamma_1 s, x-\gamma_2 z) - f_0(t,x)\big)\,\mathrm{d}z\,\mathrm{d}s.$$

When applying the Taylor expansion, all terms of order up to $m-1$ in s and z vanish, thus only the summands containing the powers s^m and z^m remain. The one-dimensional modulus of continuity (37) is replaced with the variant

$$\tilde\omega\big(f_0^{(m)};\gamma|z|,x\big) = \sup\Big\{\big|f_0^{(m)}(t,y)\big| \;\Big|\; -\gamma|z| \le x-y \le \gamma|z|,\ t\in[0,T]\Big\} \quad (39)$$

which can be bounded from above exactly as in (38). The remaining part is a straightforward generalization of the one-dimensional analysis. ■

This result can now be combined with the quantitative estimates of Section 6.1 to a convergence rate for the total reconstruction error.

Theorem 3 *Let $f \in L^1_T$ satisfy the conditions of Lemma 6 and solve $\mathcal{A}f = D_c n$ for some $n \in W^{1,1}_T$. Let further the disturbed data $n^\epsilon \in L^1_T$ be as in Theorem 2. The regularization parameter $\gamma(\epsilon) = (\gamma_1(\epsilon),\gamma_2(\epsilon))$ be chosen according to $\gamma_j(\epsilon) \sim \epsilon^{s_j}$ with $0 < s_j < 1$ $(j = 1,2)$. The exponents which lead to the same asymptotics of approximation and data errors are then given by $s_j = \frac{1}{m+1}$, and the error behaves like*

$$\|f - \mathcal{A}_{\gamma(\epsilon)} n^\epsilon\|_{L^1_T} \sim \epsilon^{\frac{m}{m+1}} \quad (\epsilon \to 0)$$

for this parameter choice.

Proof The total reconstruction error has the asymptotic behavior

$$\|f - \mathcal{A}_{\gamma(\epsilon)} n^\epsilon\|_{L^1_T} \sim \epsilon^{ms_1} + \epsilon^{ms_2} + \epsilon^{1-s_1} + \epsilon^{1-s_2}$$

according to Theorem 2 and Lemma 6. The exponents of the respective terms in s_1 and s_2 are equal if $ms_j = 1 - s_j$ which is equivalent to $s_j = (m+1)^{-1}$. Inserting this value into the total error asymptotics yields the claimed behavior. ■

7 Implementation issues

After establishing and analyzing the key concept to solve the inverse problem, the focus can now be turned to specific aspects of the numerical implementation.

7.1 Choice of the mollifier

According to Theorem 1, the generating function $\bar{\delta}$ of the mollifiers has to lie in $W^{1,1}(\mathbb{R})$, and vanishing moments lead to a certain convergence rate of the approximation error according to Lemma 6. In this work, two different functions are considered: the *Gaussian mollifier* and a *truncated polynomial mollifier* with compact support.

7.1.1 Gaussian mollifier

This alternative has been successfully employed by Groh et al. (2011) to solve the inverse problem based on steady state data of the system (9)–(11). This mollifier has the generating function

$$\bar{\delta}(x) = \frac{1}{\sqrt{2\pi}} \exp\left(-\frac{x^2}{2}\right), \quad x \in \mathbb{R}. \tag{40}$$

Obviously, $\bar{\delta}$ is continuously differentiable, and since it is a positive and even function, all odd moments vanish and all even moments are positive. Hence, the Gaussian kernel satisfies the moment conditions of Lemma 5 with $m = 2$ and leads to a total error asymptotics of $\epsilon^{2/3}$ if the regularization parameter choice asymptotically fulfills $\gamma_j(\epsilon) \sim \epsilon^{1/3}$.
Since there is no closed expression for $\Psi^x_{\gamma_2}(\xi)$, its implementation requires an adequate truncation of the series in (29) and its derivative. Fortunately, numerical experiments have revealed that after at most 20 addends there is no change in the digits of the sum value even in double precision and by summation in reverse order. This allows for a fast and stable computation of the reconstruction kernel.

7.1.2 Truncated polynomial mollifier

Amongst various alternatives, the mollifier with the compactly supported generating function

$$\bar{\delta}(v) = \frac{15}{16} \max\{(1-x^2)^2, 0\} \tag{41}$$

has been suggested by Schuster (2007). An elementary calculation shows that $\bar{\delta} \in \mathcal{C}_0^1(\mathbb{R})$ and that this kernel is of the same order $m = 2$ as the Gaussian function. The corresponding reconstruction kernel in (29) and its derivative are represented by sums with a maximum of $\left\lfloor \log\left(\frac{u+\gamma}{v}\right) / \log(2) \right\rfloor + 1$ non-vanishing terms. In addition, the reconstruction kernel in (29) inherits the compact support property from the mollifier since for fixed u, there is a v_* such that for all $v > v_*$ and $k \geq 1$, it holds $\left|u - 2^k v\right| > \gamma$, which means that $\delta_\gamma^u\left(2^k v\right) = 0$ according to (41).

7.2 Data preprocessing

As stated in Section 2, the actual task is to determine the birth rate b from discrete measurements of the number distribution. From a mathematical viewpoint, the challenging part is to reconstruct the auxiliary function f defined as the product of n and b. Once f has been computed, b can be obtained by pointwise division (see (21)):

$$b(t,x) = f(t,x)/n(t,x). \tag{42}$$

However, especially for values $n(t,x) \approx 0$ a significant noise amplification is observable such that a data smoothing can be viewed as compulsory to stabilize the determination of b according to (42). Moreover, as detailed by Groh et al. (2011), it is beneficial to employ the adequately preprocessed data already for the computation of f_γ.

It is widely known that there are several alternatives in the choice of a function approximation or regression scheme. Groh et al. (2011) successfully apply an approximation in a reproducing kernel Hilbert space with radial Wendland kernels (Wendland, 2005) to smooth a univariate histogram. On the one hand, with this technique, it is easy to incorporate certain a priori information about the data like boundary values or the asymptotics of the data function. On the other hand, a rigorous error analysis in the above mentioned article has revealed a strategy to select the adequate regularization parameter γ.

In this paper, the data function n is bivariate, which suggests the use of an accordant approximation scheme. However, in practical applications it is technically not possible to gather data sets at many points in time. For instance, relevant time series measurements as illustrated by Banks et al. (2011) show that the number of sample points in the direction of the size variable is very large compared to the time axis. Thus, the data points in the t-x plane are located along a small number of line segments parallel to the x axis. Hence, for fixed t, the data preprocessing of Groh et al. (2011) is adopted, such that

merely a smoothing in the direction of the size variable is implemented. Since the corresponding algorithm is detailed there, the interested reader is referred to this article (see also the textbook of Wendland (2005) for a comprehensive introduction). In addition, other data smoothing techniques, for example, Savitzky-Golay filters, spline smoothing, etc. would also be applicable as the good performance of the reconstruction scheme does not originate from the specific choice of the regression method. This is briefly discussed in Section 9. In the following, whenever the approximated data function n is considered, this quantity itself as well as the corresponding reconstructions f_γ and b_γ are additionally indexed with a μ.

7.3 Numerical solution of the forward problem

In order to test input data for the reconstruction method, the forward problem has to be solved. In particular, the function n is to be determined as a numerical solution of the system (9)–(11) for given rates b, c and initial value n_0.

Remark 1 Since the purpose of the numerical tests does not consist in the model evaluation but rather in the assessment of the regularization and approximation properties of the introduced inversion scheme, the data are simulated with the simplified set of equations (9)–(11).

In this paper, the explicit finite difference method introduced by Mantzaris et al. (1999), a combination of the Leapfrog and the Lax-Friedrichs schemes, is adjusted to the current problem. Accordingly, the domain $[0,T]\times[0,x_{\max}]$ is equidistantly discretized by the grid $\left\{\,(t_k,x_i)\,|\,k=1,\ldots,K+1,\ i=1,\ldots,I+1\right\}$ with $t_k=(k-1)\Delta t$, $x_i=(i-1)\Delta x$ and step sizes $\Delta t=T/K$, $\Delta x=x_{\max}/I$. The involved grid functions are defined as

$$c_i=c(x_i)\quad,\quad b_i^k=b(t_k,x_i)$$

for the given rates c, b. The scheme has been designed to compute approximations

$$n_i^k\approx n(t_k,x_i)$$

for the searched-for quantity n. The recurrence formula for the numerical solution of (9)–(11) calculates as

$$n_{i+1/2}^{k+1/2}=\frac{1}{2}\left(n_{i+1}^k+n_i^k\right)-\frac{\Delta t}{2\Delta x}\left(c_{i+1}n_{i+1}^k-c_in_i^k\right)-\frac{\Delta t}{4}\left(b_{i+1}^kn_{i+1}^k+b_i^kn_i^k\right)+2\left(b_{2i+1}^kn_{2i+1}^k+b_{2i-1}^kn_{2i-1}^k\right)$$

for $i=1,\ldots,I+1$ and

$$n_i^{k+1}=n_i^k-\frac{\Delta t}{\Delta x}\left(c_{i+1/2}n_{i+1/2}^{k+1/2}-c_{i-1/2}n_{i-1/2}^{k+1/2}\right)-\Delta tb_i^kn_i^k+4b_{2i-1}^kn_{2i-1}^k$$

for $i = 2, \ldots, I+1$ with $n_1^k = 0$ and $c_{i+1/2} = (c_{i+1} + c_i)/2$, $i = 1, \ldots, I+1$. In addition, for indices exceeding the index set related to the size variable, the grid function values are set to zero,

$$n_i^k = 0 \qquad \text{for } i > I+1,$$

which is in accordance with the asymptotic behavior of n for large x values.

8 Numerical results

8.1 Test problems

This subsection addresses the concrete specification of the system (9)–(11), the parameters of the solution scheme for the forward problem and the disturbation of the data.
In analogy to Groh et al. (2011), values of n having size argument $x \in [0, L]$ with $L = 4$ serve as input or the reconstruction procedure. However, to take the dilated term in (9) into account, the forward problem is solved on the extended domain $[0, 2L]$ and the values at points $x \in (L, 2L]$ are neglected afterwards. The temporal domain is set to $[0, T]$ for a $T > 0$ as before.
The initial value in (10) is chosen to be

$$n_0(x) = \bar{n} x \mathrm{e}^{-x^2} \quad \text{for } x \in [0, 2L],$$

since this function exhibits adequate boundary values

$$n_0(0) = 0 = \lim_{x \to \infty} n_0(x).$$

The scaling coefficient is defined as

$$\bar{n} = \left(\int_0^{2L} x \mathrm{e}^{-x^2} \, \mathrm{d}x \right)^{-1} = 2 / \left(1 - \exp(-4L^2) \right).$$

Motivated by the works of Doumic et al. (2009), Groh et al. (2011) and Doumic-Jauffret et al. (2012), the following birth rates have been designed:

$$b_{\mathrm{C}}(t, x) = 1,$$
$$b_{\mathrm{G}}(t, x) = 1 + \exp\left\{ -8 \Big(x - 1.5 + 0.5 \cos\left(2\pi t / T\right) \Big)^2 \right\},$$

where $(t, x) \in [0, T] \times [0, 2L]$. The third birth rate is a continuous, piecewise linear function with steep slopes in the direction of the x axis,

$$b_{\mathrm{L}}(t, x) = \begin{cases} 1 & , 0 \leq x \leq \xi(t), \\ 1 + m(t)\big(x - \xi(t)\big) & , \xi(t) \leq x \leq \xi(t) + 0.2, \\ h(t) & , \xi(t) + 0.2 \leq x \leq 2L, \end{cases}$$

where

$$\xi(t) = \begin{cases} 1.5 - 4\,t/T\ , 0 & \le t \le T/4, \\ -0.5 + 4\,t/T\ , T/4 & \le t \le T/2, \\ 1.5 \quad\ , T/2 & \le t \le 3T/4, \\ 4.5 - 4\,t/T\ , 3T/4 & \le t \le T, \end{cases}$$

$$m(t) = \begin{cases} 10 \quad\ , 0 & \le t \le T/2, \\ 10\,(-1 + 4\,t/T)\ , T/2 & \le t \le 3T/4, \\ 20 \quad\ , 3T/4 & \le t \le T, \end{cases}$$

$$h(t) = \begin{cases} 3 \quad\ , 0 & \le t \le T/2, \\ -1 + 8\,t/T\ , T/2 & \le t \le 3T/4, \\ 5 \quad\ , 3T/4 & \le t \le T, \end{cases}$$

The birth rates b_{G} and b_{L} are illustrated in the Figures 2 and 6, respectively. The growth rate is either chosen to be $c(x) = \alpha_0$ or $c(x) = \alpha_1 x$ with $\alpha_0, \alpha_1 > 0$. In the literature, these cases are referred to as *linear* and *exponential growth model*, respectively (Liou et al., 1997; Doumic et al., 2010). In this paper, the following values are assumed: $\alpha_0 = 1$ and $\alpha_1 = 0.1$.
With regard to the numerical solution of the system (9)–(11), the step sizes of the finite difference scheme in Subsection 7.3 are set to $\Delta x = 0.004$ and $\Delta t = \Delta x/10$. The iteration is terminated after $N = 5000$ time steps which means that $T = 2$, and, starting at $t = 0$, merely the values n_i^k for $k = 100\Delta t$ are taken into account. This reflects the fact that there is a considerable time lag between two measurements in practice. Analogously, to investigate the influence of the sampling frequency in the direction of the size variable, the spatial step size Δx is increased in some additional numerical experiments while the other parameters are kept constant. The corresponding values are given in Table 1.
In the following, the computed set of values n_i^k are denoted as *exact data*. Once these data have been generated, the values are disturbed by relative noise according to

$$n_{i,\varepsilon}^k = \max\left\{ \left(1 + \varepsilon U_{[-1,1]}\right) n_i^k\ , 0 \right\} \tag{43}$$

where $U_{[-1,1]}$ is a uniformly distributed random variable with values in $[-1, 1]$. The level of noise is governed by the parameter $\varepsilon > 0$, and the implementation of the maximum in (43) ensures non-negativity as required.
All reconstructions described in this paper have been computed on a standard PC. The routines have been implemented in MATLAB, and though the code has not been optimized, the run times for the complete reconstruction merely range from about 20 seconds to a few minutes depending on the number of data and reconstruction points. If the reconstruction kernel is precalculated, just the inner products in Theorem 1 have to be evaluated resulting in a further reduction of the computing time.

Table 1 Varying parameter values in the numerical experiments. The other parameters are constant and their values are given in the text. The additional index of γ_2 specifies the mollifier, C: mollifier with compact support, G: Gaussian

	Exact data	Minor noise	Strong noise
ε	0	0.01	0.125
σ	0.001	0.001	0.01
Δx	0.004/0.04	0.008	0.004
$c(x)$	$1/0.1x$	1	1
$\gamma_1/\gamma_{2,\mathrm{C}}$	0.11/0.350 (if $\Delta x = 0.004$, $c(x) = 1$)	0.20/0.290	
	0.11/0.540 (if $\Delta x = 0.04$, $c(x) = 1$)		
$\gamma_1/\gamma_{2,\mathrm{G}}$	0.11/0.047 (if $\Delta x = 0.004$, $c(x) = 1$)	0.15/0.075	0.15/0.06
	0.11/0.200 (if $\Delta x = 0.04$, $c(x) = 1$)		
	0.11/0.047 (if $\Delta x = 0.004$, $c(x) = 0.1x$)		
	0.11/0.230 (if $\Delta x = 0.04$, $c(x) = 0.1x$)		

8.2 Reconstructions with exact data

The characteristic of the data depends strongly on the growth rate c in the PBE (9). This is exemplarily illustrated in Figure 1. The linear growth model, $c(x) = 1$, results in a rather broad maximum near $x = 0.6$. In contrast, the exponential growth model with $c(x) = 0.1x$ yields a sharp peak in the vicinity of the origin, and this extreme value, as a function of t, increases more rapidly than in the former case.
Figure 2 illustrates the birth rate b_{G} in the form of a surface plot. The adjacent image, Figure 3, shows the pointwise relative error of the reconstructed auxiliary function $f_{\mathrm{G},\gamma}$ given by

$$E_{\mathrm{rel}}(t_k, x_i) = \left| \frac{f_\gamma(t_k, x_i) - n(t_k, x_i) b(t_k, x_i)}{n(t_k, x_i) b(t_k, x_i)} \right| . \tag{44}$$

In addition, the white curves in Figure 3 indicate the so-called *trust region*. For fixed t_k, this domain defines an interval $[x_{\mathrm{L}}(t_k), x_{\mathrm{U}}(t_k)]$, and merely reconstructions at x values within this segment can be considered to be reliable. The interval limits are defined by

$$x_{\mathrm{L}}(t_k) = \min_{i=1,\ldots,I+1} \left\{ x_i \in [0, L] \,\middle|\, n_i^k \geq \beta_k \right\} , \tag{45}$$

$$x_{\mathrm{U}}(t_k) = \max_{i=1,\ldots,I+1} \left\{ x_i \in [0, L] \,\middle|\, n_i^k \geq \beta_k \right\} , \tag{46}$$

for $\beta_k > 0$. In this paper, this set of parameters is chosen according to

$$\beta_k = \sigma \cdot \max \left\{ n_i^k \,\middle|\, i = 1, \ldots, I+1 \right\} , \tag{47}$$

where in the case of exact data, 1‰ of the maximum is taken as threshold value, i.e., $\sigma = 0.001$.
The reconstructions of b_{G} in the case of the linear growth model are illustrated in Figure 4, drawing a comparison of the results for different mollifiers and for two data sampling rates. At first, it can be observed that the scheme produces good reconstructions for both mollifiers within the trust region if a sufficient

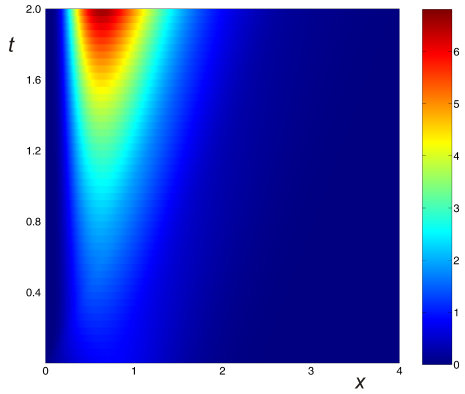

(a) Numerical solution n_{G} for the linear growth model, $c(x) = 1$

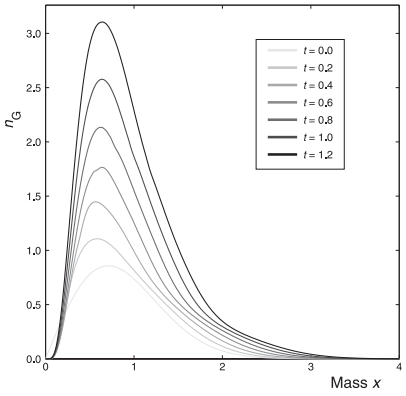

(b) Numerical solution $n_{\mathrm{G}}(t, \cdot)$ in (a) as a function of x for fixed t values

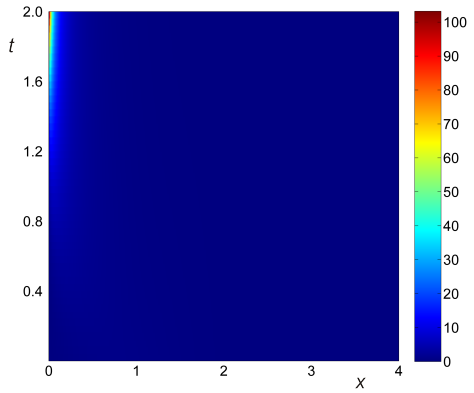

(c) Numerical solution n_{G} for the exponential growth model, $c(x) = 0.1x$

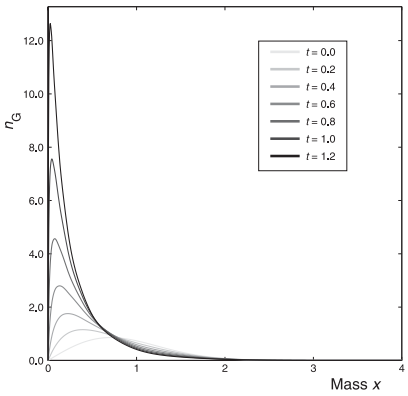

(d) Numerical solution $n_{\mathrm{G}}(t, \cdot)$ in (c) as a function of x for fixed t values

Fig. 1 Numerical solution of the initial boundary problem for growth rates $c(x) = 1$ and $c(x) = 0.1x$, respectively. In both cases the birth rate b_{G} has been employed. The parameters of the numerical experiments are given in Table 1 if not otherwise specified

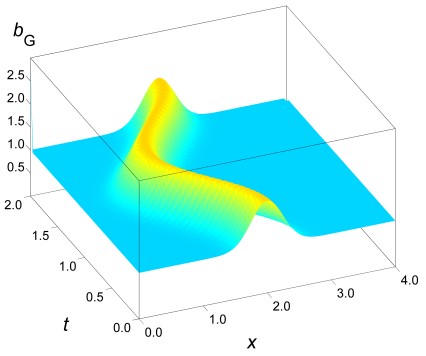

Fig. 2 Graphical representation of b_G as a surface on the t-x plane

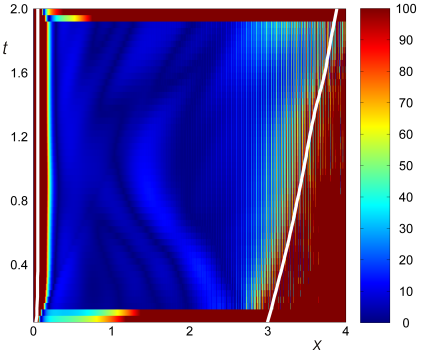

Fig. 3 Relative error of the reconstructed auxiliary function $f_{G,\gamma}$ in percent (see (44)). For a better visualization this pointwise error is bounded to 100%, i.e. "red" reflects error greater or equal to 100%. The two white curves delimit the trust region according to (45) and (46)

number of data are available. A direct juxtaposition shows that the results based on the mollifier with compact support are slightly better despite the occurrence of rapidly oscillating artifacts near the upper trust region limit x_U. Figures 4(e) and 4(f) illustrate the reconstructions if only 10% of the data points are available. The cosine function can still be identified, though the results are significantly poorer compared to the denser data set.
Finally, Figure 5 depicts the reconstructions in the case of the exponential growth model. A glance at the data visualization in Figure 1(c) suggests that the trust region has to be significantly narrower for the linear growth model. In fact, for large t, there is merely a small interval in the direction of the x axis where the reconstruction quality can be expected to be reliable. Obviously, the characteristics of this data function, namely the sharp peak and the rapid decay, pose difficulties for the reconstruction scheme.

8.3 Reconstructions with moderately disturbed data

In contrast to the preceding subsection, the presence of noise requires a preprocessing step to be applied to the data. The added relative error amounts to a maximum of 1% in this scenario, and the threshold value to define the trust region limits are the same as before, i.e., $\sigma = 0.001$. The other parameters are collected in Table 1 or can be found in Subsection 8.1. This block of experiments aims at reconstructing the piecewise linear birth rate b_L. This test function exhibits constant levels connected by steep rises in the x direction (see Figures 6(a) and 6(b)). Regarding the corresponding steady state equation of (9) considered by Doumic et al. (2009) and Groh et al. (2011), such a function is difficult to retrieve from the data. This observation transfers to the dynamical case in this paper. The corresponding results are shown in Figures

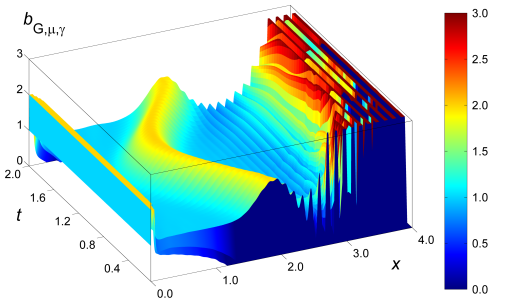

(a) Surface $b_{G,\gamma}$, where the values are adequately projected on [0,4] to improve the visualization. The reconstruction is based on data sampled at $I = 1000$ points in the x direction

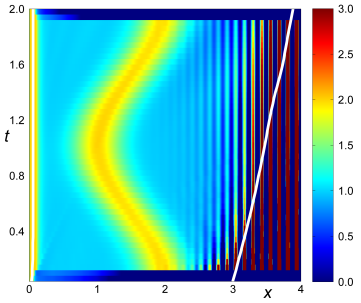

(b) Graph (a) from the bird's eye view with the trust region (white curves)

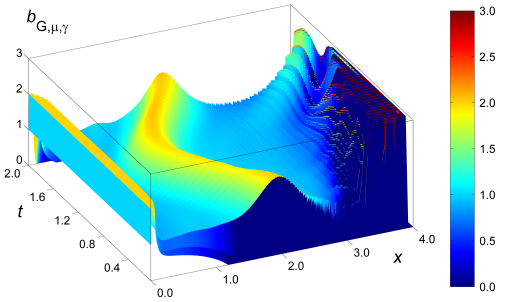

(c) Surface $b_{G,\gamma}$ with the same setup as in (a) but based on the mollifier with compact support instead of the Gaussian

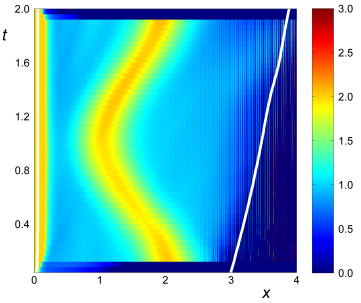

(d) Graph (c) from the bird's eye view with the trust region

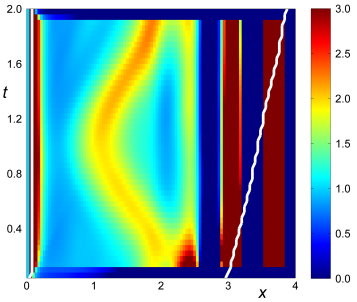

(e) The same reconstruction of b_G as in (b) with merely $I = 100$ points along the x axis

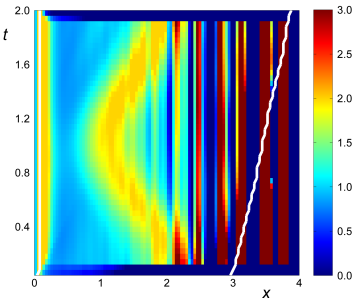

(f) The same reconstruction of b_G as in (d) with merely $I = 100$ points along the x axis

Fig. 4 First row: Reconstruction of b_G by using the Gaussian mollifier based on exact data. Second row: Reconstruction of b_G by using the mollifier with compact support. Last row: reconstruction with reduced data points (see text). In all cases, the linear growth model has been used to generate the test data sets

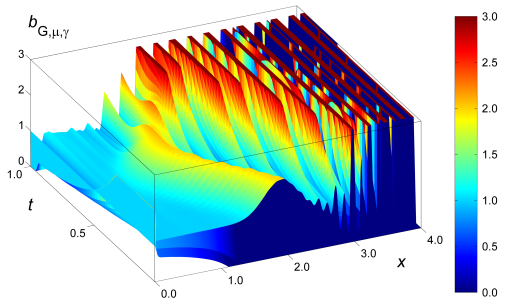

(a) Graphical representation of $b_{G,\gamma}$ as a surface on the t-x plane

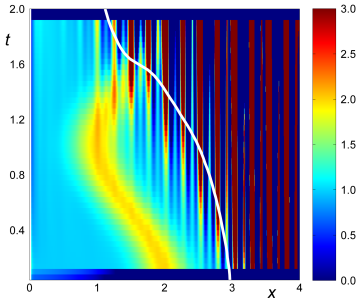

(b) Graph of (b) from the bird's eye view with the trust region (white curves)

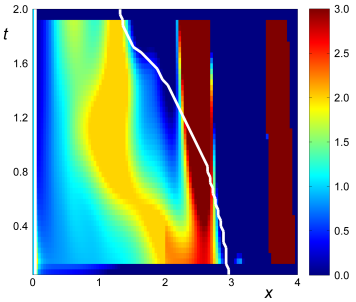

(c) Reconstruction of b_G, where merely 10% of the data have been taken into account

Fig. 5 The same illustrations as in the first row of Figure 4 (Gaussian mollifier), but for exponential growth model data

6(c) and 6(e) where either the Gaussian or the mollifier with compact support have been employed as smoothing kernels in the direction of the size variable.

Within the trust region, the essential characteristics of b_L can be recognized, though the quality is poorer compared to the preceding experiments with exact data. Regarding the performance of the two mollifiers, the reconstructions based on the Gaussian exhibit a better quality (cf. Figures 6(d) and 6(f)).

8.4 Reconstructions with strongly disturbed data

The series of experiments is completed by the consideration of strongly erroneous data $n_{C,\varepsilon}$, where the linear growth model and the constant birth rate b_C have been used in the PBE (9). The maximal pointwise relative error amounts to 12.5%, resulting in a highly oscillating data function. Some exemplary cross sections of the graph of $n_{C,\varepsilon}$ are shown in Figure 7(a), confirming the need to avoid a numerical differentiation in (12). The adjacent figure illustrates the corresponding filtered curves computed in the preprocessing step (cf. Subsection 7.2). The smoothed function $n_{C,\varepsilon,\mu}$ allows an adequate definition of the

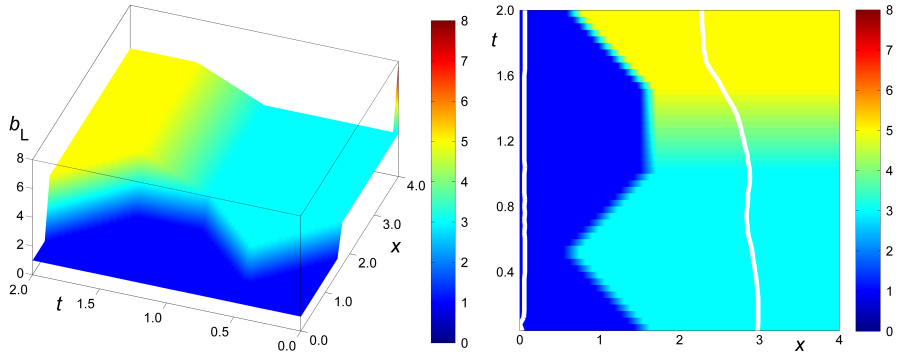

(a) Graphical representation of b_{L} as a surface on the t-x plane

(b) Graph of (a) from the bird's eye view with the trust region (white curves)

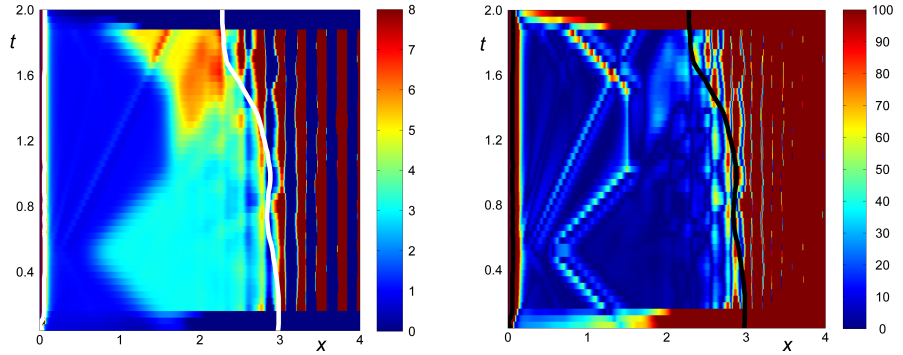

(c) Reconstruction $b_{\mathrm{L},\varepsilon,\mu,\gamma}$ with the Gaussian mollifier

(d) Projected relative error of the reconstruction in (c)

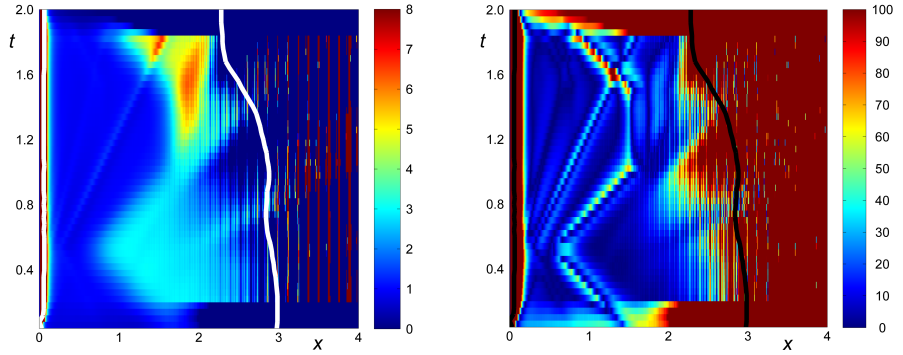

(e) Reconstruction based on the mollifier with compact support

(f) Projected relative error of the reconstruction in (e)

Fig. 6 Reconstructions from moderately disturbed data. The parameter values of the particular mollifiers are given in Table 1

trust region, where the parameter σ in (47) is adjusted to the value of 0.01 due to the high noise level.

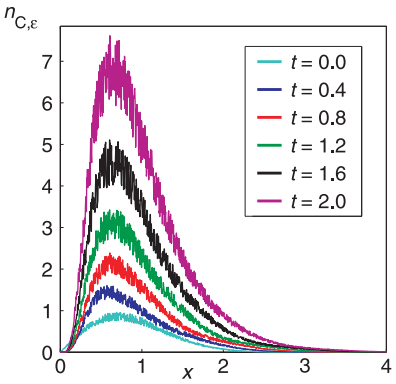

(a) Noisy number distribution $n_{C,\varepsilon}$ at fixed time instants as a function of x

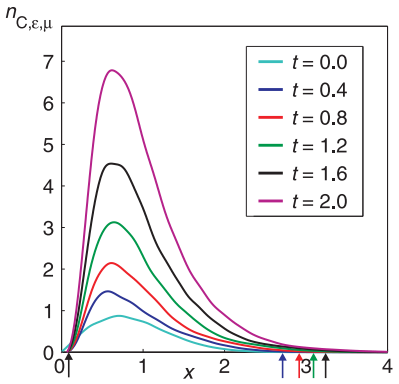

(b) Smoothed versions of the curves in (a). The limits of the trust interval are indicated by arrows of the same gray levels

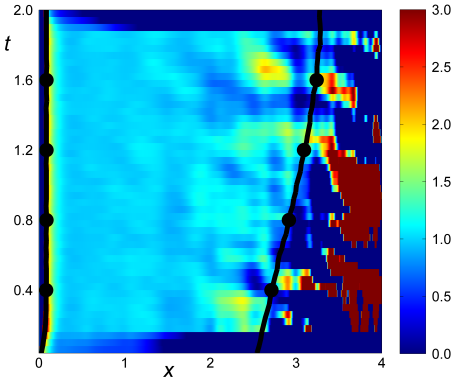

(c) Reconstruction of b_L based on the preprocessed data. The black dots on the trust region boundaries (black curves) indicate the time points $t = 0.4, 0.8, 1.2, 1.6$

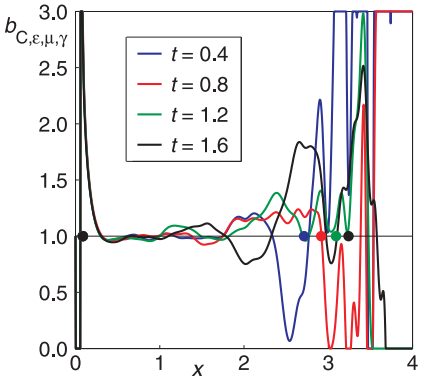

(d) Graph of the reconstruction $b_{C,\varepsilon,\mu,\gamma}$ at specific time points as a function of x

Fig. 7 Exemplary data structures in the presence of strong noise and the corresponding results based on the Gaussian mollifier acting in the x direction

Subsequent to the preprocessing step, the prepared data have been used for the reconstruction of b_C, the results of which are depicted in the Figures 7(c) and 7(d). Considering the large variance in the input data in Figure 7(a), the reconstruction within the trust region is of remarkably good quality.

8.5 Impacts of parameter variations

Step sizes Δx and Δt of the measuring system Assuming a fixed domain $[0,T] \times [0,L]$ for the data function, the fineness of the discretization plays a crucial role. As expected, starting from a coarse grid, the amount of information employed by the reconstruction scheme can be raised by a mesh refinement, leading to better results. In general, this rule is only valid up to a certain step size since a too high sampling frequency can lead to numerical instabilities due to small singular values of the forward operator.
For the sake of simplicity, the birth rates have been reconstructed at equally distributed nodes in this paper. However, according to (31), the auxiliary function can be evaluated at any arbitrary point $(t,x) \in \mathbb{R}^+ \times \mathbb{R}^+$ and the sampling of g is merely governed by the quadrature of the inner product. This can be relaxed in part by the preprocessing step (cf. Subsection 7.2).

Regularization parameters γ_1 and γ_2 The usage of two mollifiers acting in different directions is a key concept of the introduced method. This offers the opportunity to separately control the degree of smoothing along the two axes. In general, a regularization parameter balances the influence of the discretization and data errors (Louis, 1989; Engl et al., 1996), and there is a value that minimizes the global error. Groh et al. (2011) introduce an asymptotically optimal parameter choice for the Gaussian mollifier with regard to the corresponding steady state equation of (9). More precisely, the optimal value is a function of the sampling distance Δx in the direction of the x axis and it is calculated as

$$\gamma_{2,\mathrm{opt}} = \Delta x^{5/9}.$$

This concept cannot be directly adopted to the bivariate problem considered in this paper. However, it can provide a reasonable initial guess for the regularization parameter in along the x axis, which can then be fine-tuned to acquire a visually optimal result. Moreover, since there is no theoretical need for regularization along the t axis, the corresponding parameter γ_1 can be chosen in the order of the temporal sampling distance.

9 Conclusion and outlook

This paper introduces a method to approximate an unknown rate function in a size-structured PBE based on histograms of the modeled quantity at different points in time. As detailed in the introduction, such inverse problems naturally emerge in many biological applications. The standard solution techniques require an a priori discretization of the searched-for functions leading to large-scale minimization problems (Engl et al., 2009). In contrast, the introduced regularization method provides an efficient, stable and accurate alternative without a preceding projection onto a finite-dimensional function space. In addition, the implementation is rather easy and straightforward, thus it has

the potential to find its way into computer-aided real biology. In comparison with competing algorithms by Doumic et al. (2009), Doumic-Jauffret and Tine (2011), Doumic-Jauffret et al. (2012), Bourgeron et al. (2014) and Doumic and Tine (2013), the approximate inverse method requires significantly less technical effort and restrictive conditions. Moreover, the development of a numerical scheme based on the introduced approach is easier than the hybrid method that requires a combination of two regularization techniques. Finally, the application to similar data sets leads to suggestion that better results can be gained by the use of the approximate inverse method. Prior to providing an outlook on future projects, the key ideas are briefly summarized.

The initial step is to define an auxiliary function f allowing an abstraction of the problem in the form $\mathcal{A}f = g$. This suggests the application of regularization techniques established in the area of inverse problems. Compared to other schemes like the Tikhonov-Phillips method, the Landweber iteration, etc., the approximate inverse method appears beneficial for two reasons. Firstly, due to the separation approach in (24), the auxiliary problem can be reduced to the univariate equation (25) which can be solved analytically (cf. (29)). Secondly, the specific approach of the approximate inverse method allows the circumvention of the instable numerical differentiation of the noisy measurements by shifting the derivative to the given mollifier. The employed regression in a reproducible kernel Hilbert space has a supplemental stabilizing effect but this is not essential for the success of the reconstruction scheme.

In general, the approximate inverse method is formulated for unbounded domains. This can partly be made responsible for the poor results close to $x = 0$. However, the failure at the margins of the domain originates predominantly from the discrete data structure and from the underlying equation itself since the quantity $n(t, \cdot)$ exhibits a rapid decay for $x \to 0$ and for $x \to \infty$. This can be considered as a loss of information which is confirmed by the numerical experiments showing bad results at points x where $n(t, x) \approx 0$.

It should be mentioned that the cell division model (1) involves a time-independent birth rate, whereas in the numerical examples, the functions b_{G} and b_{L} were chosen to exhibit an explicit time dependence. However, they served a mere method evaluation purpose in that they represent the most general case which can be treated by the proposed scheme. Clearly, temporally constant birth rates like b_{C} are contained as special cases. It may even be considerable to apply temporal averages to a reconstructed function $b(t, x)$ in order to acquire a time-independent rate $b(x)$. This procedure, which can be expected to act additionally regularizing, requires however further investigation.

In practice, the measured histograms at specific times t_k can be fragmentary which results in a non-equidistant sampling of the number distribution $n_\varepsilon(t_k, \cdot)$ of the cell population. This circumstance does not pose any noteworthy problems since the regression method allows the evaluation of $n_{\varepsilon,\mu}(t_k, \cdot)$ at any point $x \in \mathbb{R}^+$. Though the results for noisy data simulating the situation in practical applications appear promising, the processing of real data has not yet been implemented. So far, the research efforts have been concentrated on the

algorithm development, and there has been no data interchange with biological or medical institutes yet. In this context, the introduced method can serve as a valuable tool with regard to parameter estimation and model validation in practice, especially for the aforementioned examples of biological, medical or biotechnological applications. The aim is to catch up on such interesting projects in the future.
In this paper, the model assumption of equal partitioning has led to the simplified PBE (7). The general case is the partial integro-differential equation (1). The corresponding inverse problem for the latter class of equations requires the inversion of an integral operator of the second kind. In principle, the introduced method is supposed to be applicable to this case too. However, since the auxiliary problem transforms to an integral equation of the second kind, it cannot be expected any longer to be analytically solvable. Thus, an explicit representation of the reconstruction kernel as in (29) is probably impossible, thus requiring a numerical approximation. In order to decrease the computational costs, the task is to find potential operator invariances. This allows the adaptation of the methods developed by Louis (1996) to reduce the number of evaluation points of the reconstruction kernel.

References

Abu-Absi, N. R., Zamamiri, A., Kacmar, J., Balogh, S. J., and Srienc, F. (2003). Automated flow cytometry for acquisition of time-dependent population data. *Cytometry Part A*, 51A(2):87–96.

Anderson, E. C., Bell, G. I., Petersen, D. F., and Tobey, R. A. (1969). Cell growth and division IV. Determination of volume growth rate and division probability. *Biophys. J.*, 9(2):246–263.

Arino, O. (1995). A survey of structured cell population dynamics. *Acta Biotheor.*, 43:3–25.

Banks, H. T., Sutton, K. L., Thompson, W. C., Bocharov, G., Roose, D., Schenkel, T., and Meyerhans, A. (2011). Estimation of cell proliferation dynamics using CFSE data. *Bull. Math. Biol.*, 73:116–150.

Bell, G. I. (1968). Cell growth and division III. Conditions for balanced exponential growth in a mathematical model. *Biophys. J.*, 8(4):431–444.

Bell, G. I. and Anderson, E. C. (1967). Cell growth and division I. A mathematical model with applications to cell volume distributions in mammalian suspension cultures. *Biophys J.*, 7(4):329–351.

Bourgeron, T., Doumic, M., and Escobedo, M. (2014). Estimating the division rate of the growth-fragmentation equation with a self-similar kernel. *Inverse Problems*, 30(2):025007.

Diekmann, O. (1984). The stable size distribution: an example in structured population dynamics. In *Mathematical ecology: proceedings of the autumn course (research seminars) held at the International Centre for Theoretical Physics, Miramare-Trieste, Italy, 1982*, number 54, pages 90–96.

Diekmann, O., Heijmans, H. J., and Thieme, H. R. (1984). On the stability of the cell size distribution. *J. Math. Biol.*, 19:227–248.

Diekmann, O., Lauwerier, H. A., T, T. A., and Metz, J. A. J. (1983). Growth, fission and the stable size distribution. *J. Math. Biol.*, 18:135–148.

Doumic, M. (2007). Analysis of a population model structured by the cells molecular content. *Math. Model. Nat. Phenom.*, 2(03):121–152.

Doumic, M., Maia, P., and Zubelli, J. P. (2010). On the calibration of a size-structured population model from experimental data. *Acta Biotheor.*, 58:405–413.

Doumic, M., Perthame, B., and Zubelli, J. P. (2009). Numerical solution of an inverse problem in size-structured population dynamics. *Inverse Probl.*, 25(4):045008 (25pp).

Doumic, M. and Tine, L. M. (2013). Estimating the division rate for the growth-fragmentation equation. *J Mathl Biol*, 67(1):69–103.

Doumic-Jauffret, M. and Gabriel, P. (2010). Eigenelements of a general aggregation-fragmentation model. *Math. Mod. Meth. Appl. Sci.*, 20(5):757–783.

Doumic-Jauffret, M., Hoffmann, M., Reynaud-Bouret, P., and Rivoirard, V. (2012). Nonparametric estimation of the division rate of a size-structured population. *SIAM J. Numer. Anal.*, 50(2):925–950.

Doumic-Jauffret, M. and Tine, L. M. (2011). A general inverse problem for the growth-fragmentation equation. Technical Report arXiv:1110.4798, INRIA Rocquencour.

Eakman, J. M., Fredrickson, A. G., and Tsuchiya, H. M. (1966). Statistics and dynamics of microbial cell populations. *Chem. Eng. Prog. Symp. Series*, 69(62):37–49.

Engl, H. W., Flamm, C., Kügler, P., Lu, J., Müller, S., and Schuster, P. (2009). Inverse problems in systems biology. *Inverse Probl.*, 25(12):123014 (51pp).

Engl, H. W., Hanke, M., and Neubauer, A. (1996). *Regularization of inverse problems*. Number 375 in Mathematics and its Applications. Kluwer Academic Publishers, Dordrecht.

Engl, H. W., Rundell, W., and Scherzer, O. (1994). A regularization scheme for an inverse problem in age-structured populations. *J. Math. Anal. Appl.*, 182(3):658–679.

Fredrickson, A. G., Ramkrishna, D., and Tsuchiya, H. M. (1967). Statistics and dynamics of procaryotic cell populations. *Math. Biosci.*, 1(3):327–374.

Groh, A., Krebs, J., and Wagner, M. (2011). Efficient solution of an inverse problem in cell population dynamics. *Inverse Probl.*, 27:065009 (25pp).

Gyllenberg, M. (2007). Mathematical aspects of physiologically structured populations: the contributions of J A J metz. *J. Biol. Dyn.*, 1(1):3–44.

Gyllenberg, M., Osipov, A., and Päivärinta, L. (2002). The inverse problem of linear age-structured population dynamics. *J. Evol. Equ.*, 2(2):223–239.

Gyllenberg, M., Osipov, A., and Päivärinta, L. (2003). On determining individual behaviour from population data. In Haroske, D., Runst, T., and Schmeisser, H.-J., editors, *Function spaces, differential operators, and nonlinear analysis: the Hans Triebel anniversary volume*. Birkhäuser.

Heijmans, H. J. A. M. (1984). On the stable size distribution of populations reproducing by fission into two unequal parts. *Math. Biosci.*, 72(1):19–50.

Henson, M. A. (2003). Dynamic modeling of microbial cell populations. *Curr. Opin. Biotechnol.*, 14:460–467.

Kohr, H. (2013). A linear regularization scheme for inverse problems with unbounded linear operators on Banach spaces. *Inverse Problems*, 29(6):065015.

Kolewe, M. E., Roberts, S. C., and Henson, M. A. (2012). A population balance equation model of aggregation dynamics in Taxus suspension cell cultures. *Biotechnol. Bioeng.*, 109(2):472–482.

Laurençot, P. and Perthame, B. (2009). Exponential decay for the growth-fragmentation/cell-division equation. *Commun. Math. Sci.*, 7(2):503–510.

Liou, J. J., Srienc, F., and Fredrickson, A. G. (1997). Solutions of population balance models based on a successive generations approach. *Chem. Eng. Sci.*, 52(9):1529–1540.

Liu, Y. H., Bi, J. X., Zeng, A. P., and Yuan, J. Q. (2007). A population balance model describing the cell cycle dynamics of myeloma cell cultivation. *Biotechnol. prog.*, 23(5):1198–1209.

Louis, A. K. (1989). *Inverse und schlecht gestellte Probleme*. Teubner Studienbücher Mathematik. Teubner, Stuttgart.

Louis, A. K. (1996). Approximate inverse for linear and some nonlinear problems. *Inverse Probl.*, 12(2):175–190.

Louis, A. K. (2011). Feature reconstruction in inverse problems. *Inverse Probl.*, 27(6):065010 (21pp).

Louis, A. K. and Maass, P. (1990). A mollifier method for linear operator equations of the first kind. *Inverse Problems*, 6:427–440.

Luzyanina, T., Roose, D., Schenkel, T., Sester, M., Ehl, S., Meyerhans, A., and Bocharov, G. (2007). Numerical modelling of label-structured cell population growth using CFSE distribution data. *Theor. Biol. Med. Model.*, 4(26).

Mancuso, L., Liuzzo, M. I., Fadda, S., Pisu, M., Cincotti, A., Arras, M., Nasa, G. L., Concas, A., and Cao, G. (2010a). In vitro ovine articular chondrocyte proliferation: experiments and modelling. *Cell Prolif.*, 43(3):310–320.

Mancuso, L., Scanu, M., Pisu, M., Concas, A., and Cao, G. (2010b). Experimental analysis and modelling of in vitro HUVECs proliferation in the presence of various types of drugs. *Cell Prolif.*, 43(6):617–628.

Mantzaris, N. V., Liou, J. J., Daoutidis, P., and Srienc, F. (1999). Numerical solution of a mass structured cell population balance model in an environment of changing substrate concentration. *J. Biotechnol.*, 71(1-3):157–174.

Metz, J. A. J. and Diekmann, O. (1986). The dynamics of physiologically structured populations. *Lecture notes in biomathematics*, 68.

Michel, P. (2006a). Existence of a solution to the cell division eigenproblem. *Math. Mod. Meth. in Appl. Sci.*, 16(Suppl. Issue 1):1125–1154.

Michel, P. (2006b). Optimal proliferation rate in a cell division model. *Math. Model. Nat. Phenom.*, 1(2):23–44.

Michel, P., Mischler, S., and Perthame, B. (2005). General relative entropy inequality: an illustration on growth models. *J. Math. Pure Appl.*, 84(9):1235–

1260.

Perthame, B. (2006). *Transport Equations in Biology*. Frontiers in Mathematics. Birkhäuser, Basel.

Perthame, B. and Ryzhik, L. (2005). Exponential decay for the fragmentation or cell-division equation. *J. Differ. Equations*, 210(1):155–177.

Perthame, B. and Zubelli, J. P. (2007). On the inverse problem for a size-structured population model. *Inverse Probl.*, 23(3):1037–1052.

Pilant, M. and Rundell, W. (1991a). Determining a coefficient in a first-order hyperbolic equation. *SIAM J. Appl. Math.*, 51(2):494–506.

Pilant, M. and Rundell, W. (1991b). Determining the initial age distribution for an age structured population. *Math. Popul. Stud.*, 3(1):3–20.

Ramkrishna, D. (2000). *Population balances: theory and applications to particulate systems in engineering*. Academic Press, San Diego, CA.

Ramkrishna, D., Fredrickson, A. G., and Tsuchiya, H. M. (1968). On relationships between various distribution functions in balanced unicellular growth. *Bull. Math. Biol.*, 30:319–323.

Rieder, A. and Schuster, T. (2000). The approximate inverse in action with an application to computerized tomography. *SIAM journal on numerical analysis*, 37(6):1909–1929.

Rieder, A. and Schuster, T. (2003). The approximate inverse in action II: convergence and stability. *Mathematics of computation*, 72(243):1399–1415.

Rundell, W. (1989). Determining the birth function for an age structured population. *Math. Popul. Stud.*, 1(4):377–395.

Rundell, W. (1993). Determining the death rate for an age-structured population from census data. *SIAM J. Appl. Math.*, 53(6):1731–1746.

Schuster, T. (2007). *The Method of Approximate Inverse: Theory and Applications*, volume 1906 of *Lecture Notes in Mathematics*. Springer, Berlin-Heidelberg-New York.

Schuster, T. and Schöpfer, F. (2010). Solving linear operator equations in Banach spaces non-iteratively by the method of approximate inverse. *Inverse Probl.*, 26(8):085006 (19pp).

Sidoli, F. R., Mantalaris, A., and Asprey, S. P. (2004). Modelling of mammalian cells and cell culture processes. *Cytotechnology*, 44(1):27–46.

Sinko, J. W. and Streifer, W. (1967). A new model for age-size structure of a population. *Ecology*, 48(6):910–918.

Sinko, J. W. and Streifer, W. (1969). Applying models incorporating age-size structure of a population to daphnia. *Ecology*, 50(4):608–615.

Sinko, J. W. and Streifer, W. (1971). A model for population reproducing by fission. *Ecology*, 52(2):330–335.

Subramanian, G., Ramkrishna, D., Fredricksson, A. G., and Tsuchiya, H. M. (1970). On the mass distribution model for microbial cell populations. *Bull. Math. Biol.*, 32:521–537.

Tsuchiya, H. M., Fredricksson, A. G., and Aris, R. (1966). Dynamics of microbial cell populations. *Adv. Chem. Eng.*, 6:125–206.

Webb, G. F. (2008). Population models structured by age, size, and spatial position. In *Structured Population Models in Biology and Epidemiology*,

volume 1936 of *Lecture Notes in Mathematics*, pages 1–49. Springer, Berlin, Heidelberg.

Wendland, H. (2005). *Scattered data approximation*. Cambridge University Press, Cambridge, UK, first edition.

Yosida, K. (1995). *Functional analysis. Reprint of the sixth (1980) edition. Classics in Mathematics*, volume 11. Springer.